Thermodynamics of coherent interfaces under mechanical stresses. II. Application to atomistic simulation of grain boundaries

T. Frolov* and Y. Mishin†

Department of Physics and Astronomy, MSN 3F3, George Mason University, Fairfax, Virginia 22030, USA

(Received 2 February 2012; revised manuscript received 18 May 2012; published 7 June 2012)

The thermodynamic theory of coherent interfaces developed in Part I of this work is applied to grain boundaries (GBs) subject to nonhydrostatic elastic deformations. We derive expressions for the GB free energy as the reversible work of GB formation under stress. We also present a generalized adsorption equation whose differential coefficients define the GB segregation, GB stress tensor, GB excess volume, and GB excess shear. The generalized adsorption equation generates a set of Maxwell relations describing cross effects between different GB properties. The theory is applied to atomistic simulations of a symmetrical tilt GB in Cu and Cu-Ag alloys. Using a combination of molecular dynamics and Monte Carlo methods, we compute a number of GB excess quantities and their dependencies on the applied stresses, temperature and chemical composition in the grains. We also test several Maxwell relations and obtain excellent agreement between the theory and simulations.

DOI: 10.1103/PhysRevB.85.224107 PACS number(s): 64.10.+h, 64.70.K−, 68.35.Md

I. INTRODUCTION

Solid-solid interfaces are important elements of materials microstructure. They can strongly affect thermodynamic stability of materials, phase transformations and many physical and mechanical properties.[1,2] In Part I of this work,[3] we developed a thermodynamic theory of coherent interfaces in multicomponent systems subject to nonhydrostatic mechanical stresses. Coherent interfaces were defined as those whose formation and motion conserves lattice sites and which support static shear stresses applied parallel to the interface plane. For such interfaces, we derived thermodynamic equations for the interface free energy γ as an excess of appropriate thermodynamic potentials. We also derived a generalized adsorption equation, along with its Gibbs-Helmholtz form, which are the fundamental equations of interface thermodynamics. The generalized adsorption equation naturally led us to definitions of the interface stress tensor, the interface excess volume, the excess shear and a number of other measurable excess quantities. It also generated a set of Maxwell relations describing interesting cross effects.

The goal of Part II of this work is to apply the theory of Ref. 3 to atomistic simulations of coherent grain boundaries (GBs). GBs are interfaces between regions of the same crystalline phase with different lattice orientations. Similarly to coherent phase boundaries, coherent GBs can support not only stresses normal to their plane but also shear stresses parallel to it. When a coherent GB moves, it conserves the number of lattice sites and only rearranges them from one crystallographic orientation to the other. If a GB can be equilibrated under applied stresses, the grains generally end up in different thermodynamic states due to elastic anisotropy of the lattice. In particular, their equilibrium chemical compositions and strain energy densities can be generally different. In such cases, the GB can be formally treated as simply a particular case of a phase boundary and our theory[3] applies without modifications. However, there are certain crystallographic symmetries and types of applied loads that leave the grains thermodynamically identical. The exact definition of "thermodynamically identical" grains and the corresponding symmetries were discussed in Part I.[3] In such cases, the two grains are parts of a *single* phase and all thermodynamic equations must be modified accordingly. The equations take simpler forms, which facilitates their testing by simulations. At the same time, this relatively simple case preserves most of the key concepts and relations of the general theory,[3] including the adsorption equation, the excess volume, excess shear, interface stress, and most of the Maxwell relations. Thus this case offers a convenient test bed of our theory.

In Sec. II, we discuss symmetry requirements imposed on GBs that preserve the grain identity under stresses and specialize the general thermodynamic relations of Ref. 3 to this case. In Sect. III, we introduce our simulation methodology and provide computational details. The results of the simulations are reported in Sec. IV, which is the central part of this work. The results include the effects of deformation, temperature and chemical composition of the GB free energy and GB stress. We also test several Maxwell relations that characterize mechanical, mechanochemical, thermomechanical and thermochemical responses of the boundary. In Sec. V, we summarize our work and draw conclusions.

II. THERMODYNAMICS OF GRAIN BOUNDARIES

A. Grain-boundary symmetry considerations

When the grains separated by a GB are stress free, they are thermodynamically identical and form a single-phase system. As mentioned above, when a stress is applied to the GB, it generally destroys the initial equilibrium between the grains due to elastic anisotropy of the lattice. The system can reach a new equilibrium state, but the states of the grains generally become nonidentical. We are interested in different cases, namely, in special cases when the applied stresses do preserve the single-phase nature of the system.

As an example, consider a coherent symmetrical tilt GB shown schematically in Fig. 1. Suppose the tilt axis of the boundary is aligned parallel to the Cartesian axis x_1 while the GB plane is normal to the axis x_3. Due to the mirror symmetry across the GB plane, homogeneous tensions, compressions, and in-plane shears parallel to the GB plane preserve the thermodynamic identity of the grains. The same

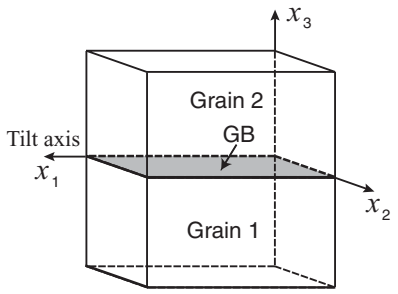

FIG. 1. Geometry of a symmetrical tilt GB relative to the coordinate axes.

is true for tensions and compressions normal to the GB plane. Furthermore, due to the twofold symmetry around the x_2 axis, the shear stress σ_{31} parallel to the tilt axis also leaves the grains identical. The only remaining stress component is the shear σ_{32} applied normal to the tilt axis. This stress can cause GB migration coupled to shear deformation of the grains.[4] Hypothetically, this migration could be stopped by creating different chemical compositions in the grains and thus an additional thermodynamic driving force opposing the coupled motion. However, even if that happened, the difference in chemical compositions would destroy the thermodynamic identity of the grains and the single-phase treatment of the GB would be impossible. To summarize, we can elastically deform a bicrystal with a symmetrical tilt boundary and still treat the two grains as a single phase as long as we keep $\sigma_{32} = 0$.

There can be other boundaries permitting single-phase treatment under applied stresses. For example, a twist boundary produced by rotation of two cubic lattices around a common [110] axis contains two mutually perpendicular two-fold symmetry axes lying in the GB plane. Suppose these symmetry axes are aligned with the coordinate axes x_1 and x_2. Then the system preserves the single-phase state when it is subject to homogeneous lateral deformations, normal tension or compression, and either $\sigma_{31} \neq 0$ with $\sigma_{32} = 0$ or $\sigma_{32} \neq 0$ with $\sigma_{31} = 0$. While such twist boundaries could be the subject of future work, in this paper, we chose a simpler and better studied case of a symmetrical tilt GB.

In the equations presented in this section, we include all stress components with the understanding that in applications to a particular GB some of them may disappear due to symmetry restrictions.

B. The grain-boundary free energy

To simplify the exposition, we will focus on a binary substitutional solid solution whose chemical composition will be characterized by the atomic fraction, c_2, of component 2. An extension to multicomponent systems with both substitutional and interstitial atoms is straightforward by analogy with Part I.[3] Vacancies are neglected and c_2 can be interpreted as the fraction of lattice sites occupied by atoms 2. This solid solution has eight thermodynamic degrees of freedom which can be, for example, the temperature T, composition c_2, and six components of the stress tensor σ_{ij}.

Following Gibbs,[5] we define the GB free energy γ as the reversible work required for creation of a unit GB area. To express γ through other thermodynamic properties, we

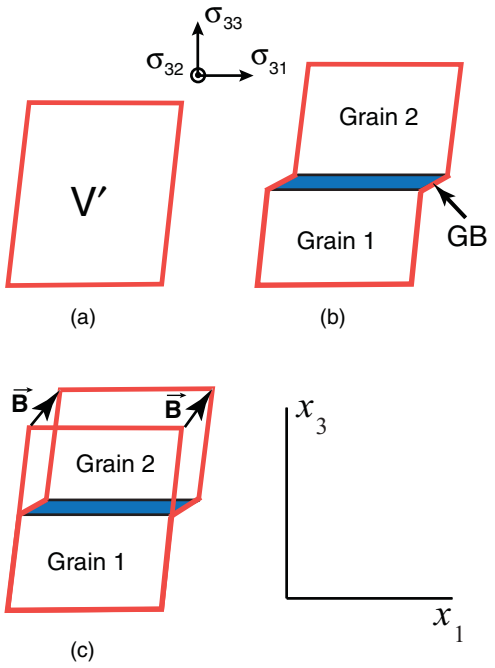

FIG. 2. (Color online) Two-dimensional schematic of the formation of a coherent GB from a single crystal. (a) Initial single-phase region of volume V'. (b) Bicrystal created by lattice transformation to a new orientation above a plane normal to x_3. (c) Overlapping shapes of the initial and final regions, showing the displacement vector **B**. This two-dimensional schematic does not show the shear deformation normal to the page.

consider a thought experiment in which the GB is formed starting from a single-crystalline sample. The GB formation process is illustrated by a two-dimensional schematic in Fig. 2. The initial state of the system is an infinitely large single crystal, in which we select a region of volume V' with the shape of a parallelepiped. The top and bottom faces of the parallelepiped are and always remain normal to the x_3 axis. This single crystal is in internal equilibrium at uniform values of the temperature, composition, and stress.

To create a tilt GB, we reversibly transform the lattice above a chosen plane normal to the x_3 axis to a new crystallographic orientation. The shape of the upper part of the selected region, which now becomes part of the upper grain, undergoes a shear deformation parallel to the GB plane (x_1,x_2). The process is also accompanied by a tensile or compressive deformation normal to the x_3 axis. During this process, the cross-section of the region parallel to the GB plane remains fixed in order to maintain the coherency. Suppose the lattice of the lower grain is fixed in space. Then, as a result of the GB formation, the lattice sites near the upper face of the parallelepiped undergo a displacement by a vector **B** shown in Fig. 2. This vector will appear in the subsequent thermodynamic equations because it defines the mechanical work W_m performed by the stress σ_{ij} during the GB formation.

As in Part I,[3] we assume that the GB formation occurs at fixed values of T, σ_{3i}, and the diffusion potential[6,7] M_{21} of component 2 relative to component 1. The system is open and its average chemical composition is allowed to vary (subject to the conservation of sites). The system can also

exchange heat with the environment. In the final state, the grains are thermodynamically identical and thus have the same temperature, chemical composition and stress as in the initial single crystal. The energy change ΔU of the discussed region is the sum of the heat $T\Delta S$, the chemical work $M_{21}\Delta N_2$, the mechanical work $W_m = A\Sigma_i B_i\sigma_{3i}$, and the nonmechanical work $W_{nm} = \gamma A$ expended for the formation of the GB. Here, A is the GB area, ΔS is the entropy change of the region, and ΔN_2 is the change in the number of atoms 2. The first law of thermodynamics leads to the following expression for γA:[3]

$$\gamma A = \Delta U - T\Delta S - M_{21}\Delta N_2 - A\sum_{i=1,2,3} B_i\sigma_{3i}. \quad (1)$$

This equation can be rewritten in a form which is more convenient for atomistic simulations. Namely, ΔU can be computed as

$$\Delta U = U - N(U_g/N_g), \quad (2)$$

where U is the total energy of the region containing the GB, N is the total number of atoms in this region, and the quantities U_g and N_g refer to an *arbitrarily chosen* homogeneous region inside one of the grains (hence the subscript g). More generally, for any extensive property Z, we introduce the notation

$$[Z]_N := Z - N(Z_g/N_g). \quad (3)$$

The meaning of $[Z]_N$ is the GB excess of property Z relative to a homogeneous grain region comprising the same total number of atoms as the region containing the boundary. For example, the excess $[N_2]_N$ characterizes the GB segregation of component 2. It can be shown that the excess quantities defined by Eq. (3) do not depend on the choice of the boundaries of the two regions (with and without the GB) involved in the calculation.[3,8]

It should be emphasized that the above definition of excesses is different from the one introduced by Gibbs, which was based on the construct of the dividing surface.[5] In the latter case, the two regions used in the excess calculation have the same volume but generally contain different numbers of atoms. Accordingly, the Gibbsian excess volume of any interface is zero by definition. The excess defined by Eq. (3) retains the GB excess volume, an important property which was measured both experimentally[9–11] and in simulations.[12–14]

Using this definition of excess quantities, Eq. (1) finally becomes

$$\gamma A = [U]_N - T[S]_N - M_{21}[N_2]_N - \sigma_{33}[V]_N - A\sum_{i=1,2} B_i\sigma_{3i}. \quad (4)$$

Note that in the mechanical work term, we separated the contributions from $i = 1$, 2, and 3. This produced a separate term containing the GB excess volume $[V]_N = AB_3$ and two terms representing the work of the shear stresses σ_{31} and σ_{32}, respectively. The coefficients AB_1 and AB_2 appearing in the last two terms are the excess shears of the boundary. Such shears exist only for coherent interfaces and were discussed in detail in Ref. 3.

Equation (4) is a particular case of Eq. (96) of Part I.[3] It clearly shows that the free energy of a GB subject to an applied stress includes the work performed by the stress during the boundary formation. In the particular case when the grains are stressed hydrostatically, the terms with σ_{31} and σ_{32} disappear. Furthermore, in hydrostatic systems $M_{21} = \mu_2 - \mu_1$, where μ_i are chemical potentials of the components. (While undefined in nonhydrostatically stressed solids,[5] chemical potentials are well-defined quantities under hydrostatic conditions.) Equation (4) then becomes

$$\begin{aligned}\gamma A &= [U - TS + pV - \mu_1 N_1 - \mu_2 N_2]_N \\ &= U - TS + pV - \mu_1 N_1 - \mu_2 N_2, \end{aligned} \quad (5)$$

where $p := -\sigma_{33}$ is pressure inside the grains and we used the relation $U_g - TS_g + pV_g - \mu_1 N_{1g} - \mu_2 N_{2g} = 0$ for homogeneous hydrostatic systems. Equation (5) recovers Gibbs' expression for γA in fluid systems.[5]

C. The adsorption equation

The adsorption equation of an interface expresses the differential of γA in terms of differentials of independent intensive variables defining the equilibrium state of the system. It is the fundamental equation of the interface, from which all other interface properties we can be derived. The adsorption equation of a GB subject to applied stresses was derived in Part I[3] as a particular case of the general coherent interface theory when the two phases are thermodynamically identical. Without repeating the derivation, we will adapt Eq. (93) from Ref. 3 for the particular case considered here:

$$\begin{aligned} d(\gamma A) = &-[S]_N dT - [N_2]_N dM_{21} - [V]_N d\sigma_{33} \\ &- A\sum_{i=1,2} B_i d\sigma_{3i} + A\sum_{i,j=1,2} \tau_{ij} de_{ji}. \end{aligned} \quad (6)$$

The last sum in this equation contains the symmetrical 2×2 lateral strain tensor de_{ji} describing elastic stretching (de_{11} and de_{22}) and shearing (de_{12}) of the boundary. It is a small-strain tensor relative to the current state of the boundary. The coefficients in front of de_{ji} describe the effect of the lateral strains on the total GB free energy γA. Tensor τ_{ij} is called the *GB stress tensor* and is similar to the interface stress discussed by Gibbs for solid-fluid interfaces.[5] Gibbs distinguished between the reversible work of interface formation, represented by γ, and the reversible work of elastic deformation of the interface, represented by interface stress. For solid-fluid interfaces, the components of τ_{ij} turn out to be quite different from γ and can be positive or negative.[15] The same is expected to be true for the GB stress.

As other coefficients in Eq. (6), the GB stress is an excess quantity. Namely, it is the excess of lateral components of the stress tensor relative to their values inside the grains. The local stress in the GB core region is generally different from the stress σ_{ij} in the grains, creating a tensile or compressive state of the boundary core described by τ_{ij}. Adapting Eq. (95) from Ref. 3, τ_{ij} can be written in the form

$$\begin{aligned}\tau_{ij} = &\frac{1}{A}\left(\overline{\sigma}_{ij}V - \delta_{ij}\sigma_{33}V - AB_i\sigma_{3j} - \delta_{ij}\sum_{k=1,2} AB_k\sigma_{3k}\right) \\ &- \frac{N}{AN_g}(\sigma_{ij}V_g - \delta_{ij}\sigma_{33}V_g). \end{aligned} \quad (7)$$

Here, δ_{ij} is the Kronecker delta, $\overline{\sigma}_{ij}$ are the lateral stress components averaged over the volume V of the region containing the GB, and V_g and N_g refer to an arbitrarily chosen homogeneous region inside the grains. Equation (7) shows that, even though τ_{ij} is an excess of the lateral stress components, its calculation generally involves also the shear and normal stress components σ_{3k} ($k = 1,2,3$). This complexity of the GB mechanics is further manifested in the Maxwell relations discussed later. In the particular case when the grains are hydrostatic, the adsorption equation becomes

$$d(\gamma A) = -[S]_N dT - [N_2]_N d(\mu_2 - \mu_1) + [V]_N dp + A \sum_{i,j=1,2} \tau_{ij} de_{ji}, \quad (8)$$

with the GB stress given by

$$\tau_{ij} = \frac{V}{A}(\overline{\sigma}_{ij} + \delta_{ij} p). \quad (9)$$

The adsorption equation (6) contains eight independent differentials representing the eight degrees of freedom of the single-phase system. However, as discussed above, in order to keep the grains thermodynamically identical, certain symmetry-dictated constraints need to be imposed on the applied stresses, such as $\sigma_{32} = 0$ for symmetrical tilt boundaries. Such constraints reduce the actual number of parameters that can be varied independently.[44]

Equation (6) can be rewritten in another form by expressing $[S]_N$ from Eq. (4) and inserting it in Eq. (6). After some rearrangement, this gives

$$d\left(\frac{\gamma A}{T}\right) = -\frac{\Psi}{T^2} dT - \frac{[N_2]_N}{T} dM_{21} - \frac{[V]_N}{T} d\sigma_{33} - \frac{A}{T} \sum_{i=1,2} B_i d\sigma_{3i} + \frac{A}{T} \sum_{i,j=1,2} \tau_{ij} de_{ji}, \quad (10)$$

where

$$\Psi := [U]_N - M_{21}[N_2]_N - \sigma_{33}[V]_N - A \sum_{i=1,2} B_i \sigma_{3i}. \quad (11)$$

Equation (10) can be called the Gibbs-Helmholtz form of the adsorption equation. Its derivation is mathematically similar to the derivation of the classical Gibbs-Helmholtz equation $\partial(G/T)/\partial T = -(U + pV)/T^2$ for bulk fluid systems, G being the Gibbs free energy.[16] In fact, if all variables in Eq. (10) are fixed and only temperature is varied, this equation reduces to $\partial(\gamma A/T)/\partial T = -\Psi/T^2$ with γA playing the role of G and Ψ playing the role of the enthalpy $U + pV$.

The advantage of the Gibbs-Helmholtz form (10) over the standard form of the adsorption equation is that the former does not contain the excess entropy, the quantity which is difficult to measure or compute. This makes Eq. (10) more suitable for calculations of γ by thermodynamic integration. Indeed, all excess quantities appearing in Eq. (10) are easily accessible by atomistic simulations. Thus all differential coefficients of this equation can be readily computed along an equilibrium path connecting a chosen reference state with the state of interest. This approach to calculation of γ will be applied later in this paper.

D. The Lagrangian and physical forms of the adsorption equation

As discussed in Sec. II B (see also Part I),[3] the product γA appearing in the adsorption equations (6) and (10) is the total free energy of a GB patch within a selected region containing a fixed set of lattice sites. During the lateral deformations described by the strain tensor de_{ij}, those lattice sites are conserved and are only stretched and/or sheared elastically parallel to the GB plane. In terms of continuum mechanics,[17] this means that the Lagrangian area of the GB remains fixed whereas its Eulerian (physical) area A changes. Let the GB area in its current state, i.e. prior to the application of the strain de_{ij}, be denoted A'. Then there are two ways to define a specific GB free energy: by dividing γA by the physical (elastically deformed) area A and by dividing it by the Lagrangian area A'. The first definition gives the physical GB free energy γ, while the second gives the Lagrangian GB free energy $\gamma' := (\gamma A)/A'$.

This classification can be applied to all other excess quantities: any total excess $[Z]_N$ generates the specific excesses $[Z]_N/A$ (physical) and $[Z]_N/A'$ (Lagrangian). In particular, the GB stress τ_{ij} introduced above is the physical specific excess of the lateral stress components, whereas $\tau'_{ij} := (\tau_{ij} A)/A'$ is the corresponding Lagrangian excess. Likewise, besides the physical excess shears B_1 and B_2 we can introduce their Lagrangian counterparts $B'_1 := (B_1 A)/A'$ and $B'_2 := (B_2 A)/A'$.

To emphasize that Eqs. (6) and (10) are Lagrangian forms of the adsorption equation, they can be rewritten as

$$d\gamma' = -\frac{[S]_N}{A'} dT - \frac{[N_2]_N}{A'} dM_{21} - \frac{[V]_N}{A'} d\sigma_{33} - \sum_{i=1,2} B'_i d\sigma_{3i} + \sum_{i,j=1,2} \tau'_{ij} de_{ji} \quad (12)$$

and

$$d\left(\frac{\gamma'}{T}\right) = -\frac{\Psi}{A'T^2} dT - \frac{[N_2]_N}{A'T} dM_{21} - \frac{[V]_N}{A'T} d\sigma_{33} - \sum_{i=1,2} \frac{B'_i}{T} d\sigma_{3i} + \sum_{i,j=1,2} \frac{\tau'_{ij}}{T} de_{ji}, \quad (13)$$

where all differential coefficients are Lagrangian specific excesses. To obtain the respective physical forms of the adsorption equation, we take the differential of γA in the left-hand side and move the term γdA to the right-hand side. Using the relation $dA = A \sum_{i,j=1,2} \delta_{ij} de_{ij}$, we obtain

$$d\gamma = -\frac{[S]_N}{A} dT - \frac{[N_2]_N}{A} dM_{21} - \frac{[V]_N}{A} d\sigma_{33} - \sum_{i=1,2} B_i d\sigma_{3i} + \sum_{i,j=1,2} (\tau_{ij} - \delta_{ij}\gamma) de_{ji} \quad (14)$$

and

$$d\left(\frac{\gamma}{T}\right) = -\frac{\Psi}{AT^2} dT - \frac{[N_2]_N}{AT} dM_{21} - \frac{[V]_N}{AT} d\sigma_{33} - \sum_{i=1,2} \frac{B_i}{T} d\sigma_{3i} + \sum_{i,j=1,2} \frac{(\tau_{ij} - \delta_{ij}\gamma)}{T} de_{ji}. \quad (15)$$

As for phase boundaries,[3] Eqs. (12) and (14) generate the Lagrangian form of the Shuttleworth equation,[8]

$$\frac{\partial \gamma'}{\partial e_{ij}} = \tau'_{ij}, \tag{16}$$

as well as its physical form,[18]

$$\frac{\partial \gamma}{\partial e_{ij}} = \tau_{ij} - \delta_{ij}\gamma. \tag{17}$$

E. Maxwell relations

All forms of the adsorption equation discussed above express $d\gamma, d(\gamma A), d(\gamma/T)$ and $d(\gamma A/T)$ as perfect differentials of intensive variables. These equations generate a number of Maxwell relations between their differential coefficients. Since these differential coefficients are either Lagrangian or physical excesses, each Maxwell relation can be written in two forms: Lagrangian and physical. The preferred choice of the form depends on the case. For example, in Maxwell relations involving the GB stress, the Lagrangian form contains the readily accessible tensor τ'_{ij}, whereas the physical form contains the quantity $(\tau_{ij} - \delta_{ij}\gamma)$ whose calculation requires knowledge of γ. Because γ is difficult to compute or measure experimentally, the Lagrangian form is preferred.

A number of Maxwell relations were presented in Part I of this work.[3] For reference purposes, they are listed below in a form adapted for GBs. Each relation is given in the Lagrangian and physical forms. In some cases, when the derivatives are taken at a fixed cross section of the GB, the two forms are identical and we list only the Lagrangian form. As in Ref. 3, all relations are divided into four categories, depending on the type processes represented by the derivatives.

(i) Mechanical relations:

$$\frac{\partial \tau'_{ij}}{\partial e_{kl}} = \frac{\partial \tau'_{kl}}{\partial e_{ij}}, \quad \frac{\partial(\tau_{ij} - \delta_{ij}\gamma)}{\partial e_{kl}} = \frac{\partial(\tau_{kl} - \delta_{kl}\gamma)}{\partial e_{ij}}, \quad i,j,k,l = 1,2, \tag{18}$$

$$\frac{\partial \tau'_{ij}}{\partial \sigma_{33}} = -\frac{\partial([V]_N/A')}{\partial e_{ij}}, \quad \frac{\partial(\tau_{ij} - \delta_{ij}\gamma)}{\partial \sigma_{33}} = -\frac{\partial([V]_N/A)}{\partial e_{ij}}, \quad i,j = 1,2, \tag{19}$$

$$\frac{\partial \tau'_{ij}}{\partial \sigma_{3k}} = -\frac{\partial B'_k}{\partial e_{ij}}, \quad \frac{\partial(\tau_{ij} - \delta_{ij}\gamma)}{\partial \sigma_{3k}} = -\frac{\partial B_k}{\partial e_{ij}}, \quad i,j,k = 1,2, \tag{20}$$

$$\frac{\partial B'_k}{\partial \sigma_{33}} = \frac{\partial([V]_N/A')}{\partial \sigma_{3k}}, \quad k = 1,2. \tag{21}$$

(ii) Mechanochemical relations:

$$\frac{\partial \tau'_{ij}}{\partial M_{21}} = -\frac{\partial([N_2]_{XY}/A')}{\partial e_{ij}}, \quad \frac{\partial(\tau_{ij} - \delta_{ij}\gamma)}{\partial M_{21}} = -\frac{\partial([N_2]_N/A)}{\partial e_{ij}}, \quad i,j = 1,2, \tag{22}$$

$$\frac{\partial([V]_N/A')}{\partial M_{21}} = \frac{\partial([N_2]_N/A')}{\partial \sigma_{33}}, \tag{23}$$

$$\frac{\partial B'_k}{\partial M_{21}} = \frac{\partial([N_2]_N/A')}{\partial \sigma_{3k}}, \quad k = 1,2. \tag{24}$$

(iii) Thermomechanical relations:

$$\frac{\partial(\tau'_{ij}/T)}{\partial T} = -\frac{\partial([\Psi]_N/A'T^2)}{\partial e_{ij}}, \quad \frac{\partial\{(\tau_{ij} - \delta_{ij}\gamma)/T\}}{\partial T} = -\frac{\partial([\Psi]_N/AT^2)}{\partial e_{ij}}, \quad i,j = 1,2, \tag{25}$$

$$\frac{\partial([V]_N/A'T)}{\partial T} = \frac{\partial([\Psi]_N/A'T^2)}{\partial \sigma_{33}}, \tag{26}$$

$$\frac{\partial B'_k}{\partial T} = \frac{\partial([\Psi]_N/A'T^2)}{\partial \sigma_{3k}}, \quad k = 1,2. \tag{27}$$

(iv) Thermochemical relation:

$$\frac{\partial([N_2]_N/A'T)}{\partial T} = \frac{\partial([\Psi]_N/A'T^2)}{\partial M_{21}}, \tag{28}$$

Equations (18)–(20) describe the effect of applied stresses on the GB stress. In Eq. (19), the right-hand side describes the GB "Poisson effect," i.e, the effect of lateral strains on the GB "thickness" (excess volume per unit area). The right-hand side of Eq. (21) represents a more subtle effect, in which applied shear stresses influence the GB excess volume. The right-hand sides of Eqs. (22)–(24) describe the effect of applied lateral strains, normal stress, and shear stresses on GB segregation.

III. METHODOLOGY OF ATOMISTIC SIMULATIONS

A. Simulated systems

A bicrystal containing a symmetrical tilt $\Sigma 5$ (310) GB was created by standard geometric constructions.[19] The grains were symmetrically misoriented by 36.87° around the [001] tilt axis parallel to the x_1 direction of the coordinate system. The GB plane is (310) and is normal to the x_3 axis. The atomic structure of this boundary viewed down the tilt axis consists of identical kite-shaped structural units shown in Fig. 3. Due to the $2mm$

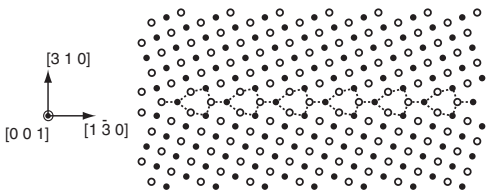

FIG. 3. Atomic structure of the symmetrical tilt $\Sigma 5$ (310) GB. The open and filled circles indicate atomic positions in alternate (002) planes parallel to the page. The tilt axis is normal to the page. The kite-shaped structural units are outlined.

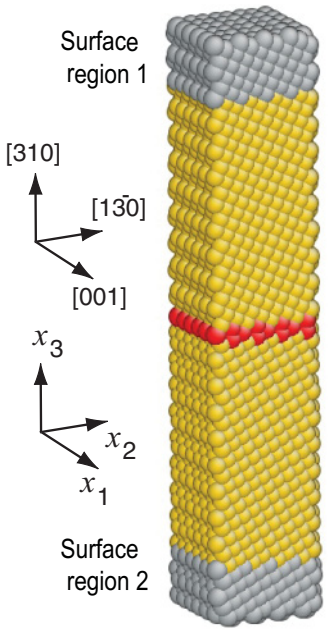

FIG. 4. (Color online) Simulation block containing the Σ5 (310) symmetrical tilt GB. The GB position is indicated by the red color. The atoms colored in grey form the surface regions 1 and 2 discussed in the text. Boundary conditions parallel to the GB plane are periodic. The image was produced with the ATOMEYE visualization program.[43]

symmetry of this boundary, uniform elastic deformations of the bicrystal create identical stress tensors in both grains and thus preserve equilibrium between them as long as the shear stress σ_{32} remains zero. A nonzero σ_{32} destroys the identity of the grains and induces coupled motion of this boundary.[4,20] It should be noted that this boundary remains coupled even at $\sigma_{32} = 0$. Its spontaneous displacements up and down are accompanied by concurrent grain translations by geometrically prescribed amounts.[4] Such coupled displacement-translation events are equilibrium fluctuations and do not contradict our thermodynamic analysis.

The simulation block had dimensions $22 \times 23 \times 145$ Å and contained 5256 atoms (see Fig. 4). Periodic boundary conditions were applied in the x_1 and x_2 directions parallel to the GB plane. In the x_3 direction, the grains terminated at "surface regions" labeled 1 and 2. The thickness of each surface region was twice the cutoff radius of atomic interactions. The motion of atoms in these regions was subject to certain restrictions which produced desired states of stress in the system. Unless otherwise stated, the atoms in region 2 are fixed in their perfect lattice positions to prevent rigid translations of the entire simulation block.

We used pure Cu and Cu-Ag alloys as model materials. Interactions between the atoms were modeled by embedded-atom method potentials for copper[21] and the Cu-Ag system.[22] The binary potential reproduces the eutectic phase diagram of the Cu-Ag system in semiquantitative agreement with experiment.[23] Cu was chosen as component 1 and Ag as component 2. The chemical composition is characterized by the atomic fraction, c_{Ag}, of Ag atoms. In this work, we studied Cu-rich solid solutions with c_{Ag} less than 1%.

B. Simulations in pure Cu

The effect of elastic deformation on GB properties in pure Cu was studied at the temperature of 0 K. Lateral deformations of the simulation block were described by a small-strain tensor e_{ij} relative to the initial state with stress-free grains. To compute the GB excess properties as functions of e_{11}, e_{22}, σ_{31}, and σ_{33} and to test the Maxwell relations (18)–(21), the GB was elastically deformed along various deformation paths. The deformations included tensions and compressions parallel to the coordinate axes and a shear parallel to the GB plane in the x_1 direction.

Uniaxial and biaxial deformations parallel to the GB plane were modeled by imposing the strains e_{11} or e_{22} (or both) while keeping the stress components σ_{31}, σ_{32}, and σ_{33} zero. For biaxial deformations, the block was strained by $e_{11} = e_{22} := e$. The deformations were implemented by scaling the atomic coordinates in small increments followed by static relaxation after each step. During the relaxation, the lateral dimensions of the system were kept fixed, allowing the atoms to move until the total energy reached a minimum. The amount of strain was varied from −1.6% (compression) to 1.6% (tension). Because the principal axes of stress and strain coincide by symmetry of the system, such deformations do not create any shear stresses σ_{31} or σ_{32}. Furthermore, atoms in the surface region 1 were allowed to move freely in the x_3 direction, imposing the zero-stress condition $\sigma_{33} = 0$.

Tension and compression normal to the GB plane were applied by scaling the x_3 coordinates of all atoms by small increments followed by static relaxation. During the relaxation, atomic positions in the surface regions 1 and 2 remained fixed. This deformation produced a normal stress σ_{33} while keeping the shear stresses σ_{31} and σ_{32} zero by symmetry. The relaxed σ_{33} values implemented in the simulations ranged form −2.4 GPa (compression) to 2.7 GPa (tension).

Finally, the shear stress σ_{31} parallel to the tilt axis was applied at fixed lateral dimensions of the simulation block and zero σ_{33}. The shear was imposed by incremental rigid displacements of surface region 1 in the x_1 direction while keeping fixed atomic positions in surface region 2. During the relaxation, the atoms in surface region 1 were allowed to move only in the x_3 direction, imposing the $\sigma_{33} = 0$ condition. Using this procedure, σ_{31} was ramped from 0 to 1.49 GPa. Changing the sign of the shear would produce identical result due to the mirror plane normal to the x_1 axis.

For calculation of excess quantities, the region containing the GB comprised all atoms separated by more than 20 Å from each of the surface regions. The grain properties were computed by averaging over two approximately 25-Å-thick homogeneous regions selected inside the grains and not influenced by the GB or the surface regions. The exact boundaries of these regions were chosen to coincide with (310) atomic planes. To calculate the relevant components of vector **B**, all atoms outside the GB core were assigned to individual (310) layers and average coordinates of atoms belonging to such layers were computed. Let (X_1, X_2, X_3) denote the average coordinates of the top layer of the region containing the GB relative to its bottom, and let (X_{1g}, X_{2g}, X_{3g}) be a similar vector computed for the selected homogeneous grain region. Then B_1 and B_3 are given by $B_i = X_i - (N/N_g)X_{ig}$, $i = 1,3$.

Testing the Maxwell relations required calculation of derivatives of GB excess quantities with respect to e_{11}, e_{22}, σ_{31}, or σ_{33}. To this end, the discrete data points obtained by individual simulations were fitted with a second-order polynomial and the derivative was evaluated for the stress-free state.

The GB properties at finite temperatures were studied by molecular dynamics (MD) simulations in the NVT ensemble (constant number of atoms N, volume V and temperature T) using the Nose-Hoover thermostat. The MD simulations employed the ITAP molecular dynamics (IMD) program[24–26] and were performed in the temperature range from 0 to 900 K in 100 K steps. At each temperature, the simulation block was pre-expanded by the thermal expansion factor computed previously[21] to eliminate thermal stresses in the grains. No restrictions were imposed on atomic motion in the surface regions 1 and 2, turning them to open surfaces. While this procedure ensured stress-free states inside the grains, finite lateral stresses σ_{11} and σ_{22} existed in the GB region due to the GB stress τ_{ij}. At each temperature, the system was equilibrated for 2 ns, followed by a 10-ns-long production run during which multiple snapshots of the system were generated. The snapshots contained positions of atoms as well as their energies and stresses. This data was later used for post-processing the results.

C. Simulations for the binary Cu-Ag system

To model the binary Cu-Ag system at finite temperatures, we used Monte Carlo (MC) simulations in the semi-grand canonical ensemble.[27–29] In this ensemble, the temperature and the total number N of atoms are fixed, whereas the positions and chemical species of the atoms can vary. Each step of the MC process includes a random selection of an atom and its small random displacement with simultaneous random change of its chemical species. The trial move is accepted or rejected according to the Metropolis algorithm. The probability of switching chemical species depends on the diffusion potential M_{21}, which is an input parameter of the simulation. The MC simulations allow the system to reach equilibrium much faster than by MD simulations, which require actual diffusion of atoms.

The MC simulations were performed at a constant temperature of 800 K and sampled the composition range from $c_{\mathrm{Ag}} = 0$ to $c_{\mathrm{Ag}} = 0.58\%$ inside the grains. Different chemical compositions in the grains were created by adjusting the value of M_{21}. Prior to each simulation, the block was pre-expanded according to the expansion coefficient of a bulk solid solution subject to the chosen M_{21}. Such expansion coefficients were computed in separate MC simulations of a single crystal with all-periodic boundary conditions in the NPT ensemble (constant number of atoms N, pressure P and temperature T) at zero pressure. This pre-expansion procedure was applied to eliminate the compositional and thermal stresses inside the grains. During the subsequent MC simulations, the x_1 and x_2 dimensions of the simulation block remained fixed, whereas in the x_3 direction the grains terminated at free surfaces. In each simulation run, the system was first equilibrated by 5×10^4 MC steps per atom, followed by a production stage which typically comprised 7×10^5 MC steps per atom. During the production run, snapshots containing energies, stresses and atomic species of individual atoms were generated every 70 MC steps per atom.

To test the Maxwell relations, four types of simulation were conducted: (i) biaxial tension/compression parallel to the GB plane at constant T, M_{21}, σ_{31}, and σ_{33}, (ii) tension/compression normal to the GB plane at constant T, M_{21}, and e, (iii) variation of M_{21} at constant T, σ_{31}, σ_{33}, and e, and (iv) variation of T at constant M_{21}, σ_{31}, σ_{33}, and e. The elastic deformations were implemented by the same methodology as in the 0 K simulations described above. In each of the four types of state variations, several MC simulations were performed at different values of the respective intensive parameter (e, σ_{33}, M_{21}, or T). Each simulation included the equilibration and production stages as indicated above and produced average values of the relevant GB properties. The discrete data points thus obtained were fitted with a second-order polynomial to compute the respective derivative. All derivatives appearing in the Maxwell relations were evaluated for the same thermodynamic state of the grains, namely, $T = 800$ K, $M_{21} = 0.4$ eV, and $\sigma_{ij} = 0$. In this state, the chemical composition inside the grains was $c_{\mathrm{Ag}} = 0.036\%$.

IV. RESULTS

A. Pure Cu at 0 K

At 0 K the entropy terms in all equations vanish and there is no need to compute the excess entropy $[S]_N$. This simplifies all thermodynamic equations and enables direct calculation of γ through appropriate excesses of energy and other quantities. Calculations at 0 K allow us to test the proposed thermodynamic integration schemes by computing γ both directly (as indicated below) and by integration of the adsorption equation. We will test several integration paths corresponding to different types of deformation. Thermodynamic integration requires knowledge of γ in a reference state. The latter was chosen to be the state with stress-free grains at 0 K. The GB free energy γ_0 in this state is readily computed by $[U]_N/A'$, where A' is the respective GB area. The calculations give $\gamma_0 = 0.905$ J/m^2 in agreement with previous work.[19]

1. Tension and compression parallel to the GB plane

The GB free energy was computed as a function of strain for two uniaxial deformations (e_{11} and e_{22}) and the biaxial deformation. Because all σ_{3i} are zero, Eq. (4) reduces to

$$\gamma = [U]_N/A, \tag{29}$$

offering an easy recipe for calculation of γ. On the other hand, the integrated forms of Eq. (6) for these deformations are

$$\gamma = \frac{\gamma_0 A'}{A} + \frac{1}{A}\int \tau_{11} A de_{11}, \tag{30}$$

$$\gamma = \frac{\gamma_0 A'}{A} + \frac{1}{A}\int \tau_{22} A de_{22}, \tag{31}$$

$$\gamma = \frac{\gamma_0 A'}{A} + \frac{1}{A}\int (\tau_{11} + \tau_{22}) A de. \tag{32}$$

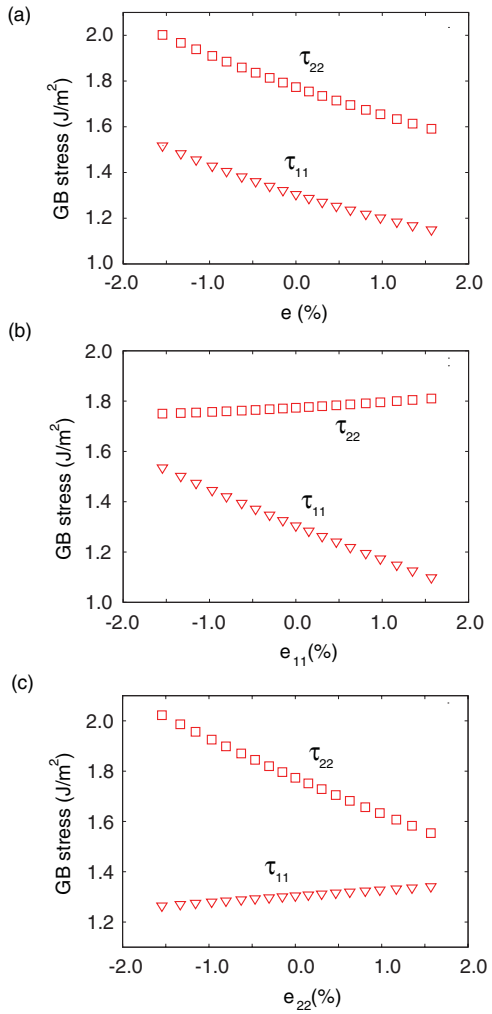

FIG. 5. (Color online) GB stress in pure Cu at 0 K as a function of strain. (a) Biaxial strain ($e := e_{11} = e_{22}$). (b) Uniaxial strain e_{11}. (c) Uniaxial strain e_{22}.

The GB stress τ_{ij} is readily computed from Eq. (7), which with $\sigma_{3i} = 0$ reduces to

$$\tau_{ii} = \frac{1}{A}\left(\overline{\sigma}_{ii}V - \frac{N}{N_g}\sigma_{ii}V_g\right), \quad i = 1,2. \tag{33}$$

By the symmetry of the system $\tau_{12} = 0$.

For the reference state ($\sigma_{ij} = 0$), the calculations give $\tau_{11} = 1.305$ J/m^2 and $\tau_{22} = 1.774$ J/m^2. During the biaxial deformation, both components of τ_{ij} decrease under tension and increase under compression (see Fig. 5). The fact that $\partial\tau_{ii}/\partial e < 0$ indicates that the GB core is "softer" than the lattice (positive excess of compliance). At all strains tested, both components of τ_{ij} remain positive, i.e., the GB core is under tension.

Figure 6 displays the plots of γ as a function of strain for all three deformation paths. The discrete points were obtained by direct calculations from Eq. (29), whereas the lines were computed by integration of Eqs. (30)–(32). The excellent agreement between the two calculations confirm the correctness and accuracy of our methodology. Note that $\partial\gamma/\partial e_{ii} > 0$, i.e., γ increases under tension and decreases under compression. Since both components of τ_{ij} are larger

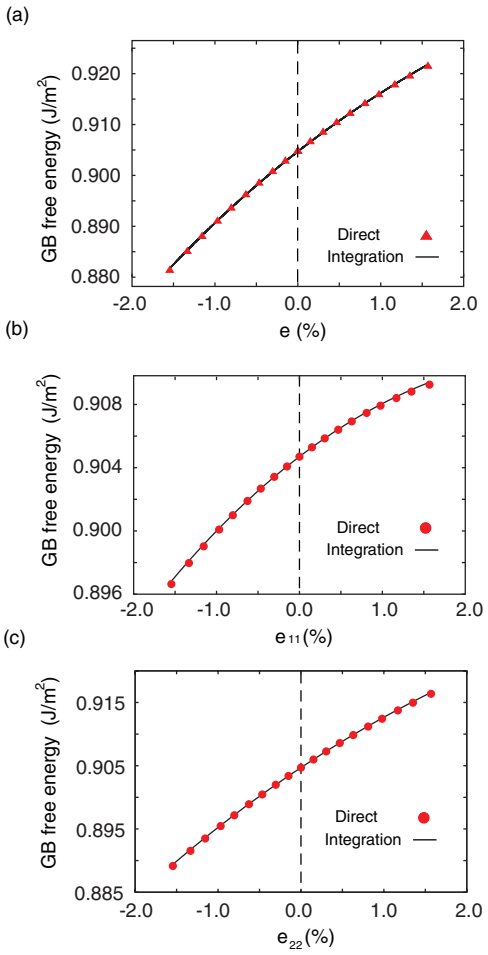

FIG. 6. (Color online) GB free energy as a function of strain for pure Cu at 0 K. (a) Biaxial strain ($e := e_{11} = e_{22}$). (b) Uniaxial strain e_{11}. (c) Uniaxial strain e_{22}.

than γ, this behavior is consistent with the Shuttleworth equation (17).

2. *Deformation normal to the GB plane*

When the GB is subject to a normal stress σ_{33}, γ is no longer identical to the excess energy. In addition to $[U]_N$, there is another term representing the mechanical work of the normal stress when the boundary is formed. Accordingly, Eqs. (4) and (6) become

$$\gamma = [U]_N/A - \sigma_{33}[V]_N/A \tag{34}$$

and

$$\gamma = \gamma_0 - \frac{1}{A}\int [V]_N d\sigma_{33}, \tag{35}$$

respectively.

The integration in Eq. (35) requires knowledge of the excess GB volume $[V]_N$ as a function of σ_{33}. This function has been calculated and is illustrated in Fig. 7 with $[V]_N$ normalized by the GB area (which remains constant during the deformation). The stress-free value of $[V]_N/A$ is 0.316 Å; it increases under tension and decreases under compression. The plot also reveals a significant tension-compression asymmetry of the

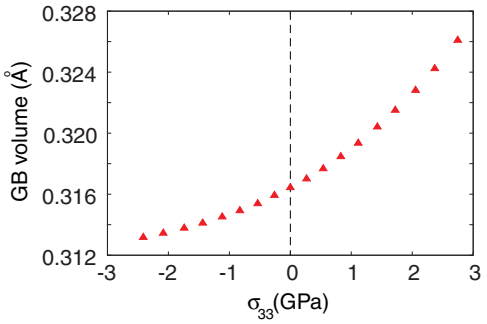

FIG. 7. (Color online) Excess GB volume per unit area, $[V]_N/A$, as a function of normal stress σ_{33}. The calculation was performed for pure Cu at 0 K.

excess volume. Namely, the GB core is elastically stiffer under compression and more compliant under tension.

Figure 8 shows the GB free energy computed directly from Eq. (34) (discrete points) and by thermodynamic integration using Eq. (35) (solid line). Again excellent agreement is observed between the two calculation methods. It is noteworthy that γ decreases under normal tension and increases under normal compression, which is consistent with the positive sign of the excess volume. The variations in γ are nearly linear in stress, which is consistent with the fact that $[V]_N$ varies with σ_{33} by only a few percent. It should be noted, however, that at the stress level of about 3 GPa neglecting the second term in Eq. (34) would produce a 10% overestimate of the GB free energy. This effect can be quite significant given that in experiment (especially in polycrystalline materials) local stresses produced in GB regions by nearby dislocations and other defects, or arising due to the concentration of applied loads, can readily reach GPa levels.

3. *Shear deformation parallel to the tilt axis*

Under a shear stress σ_{31}, all atoms have a displacement component in the x_1 direction parallel to the tilt axis. An example is shown in Fig. 9(a) where we plot the elastic displacements u_1 relative to the state with stress-free grains versus the x_3 coordinate for $\sigma_{31} = 1.5$ GPa. Each u_1 was averaged over atoms lying in the same (310) plane parallel to the GB. Observe that inside the grains u_1 is a linear function of x_3. The slope of this line represents the inverse of the

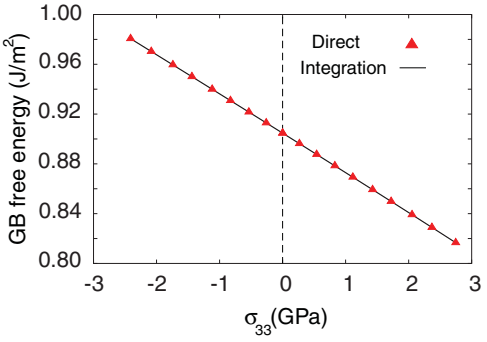

FIG. 8. (Color online) GB free energy as a function of normal stress σ_{33} for pure Cu at 0 K. The discrete points were obtained by direct calculation, while the lines by thermodynamic integration.

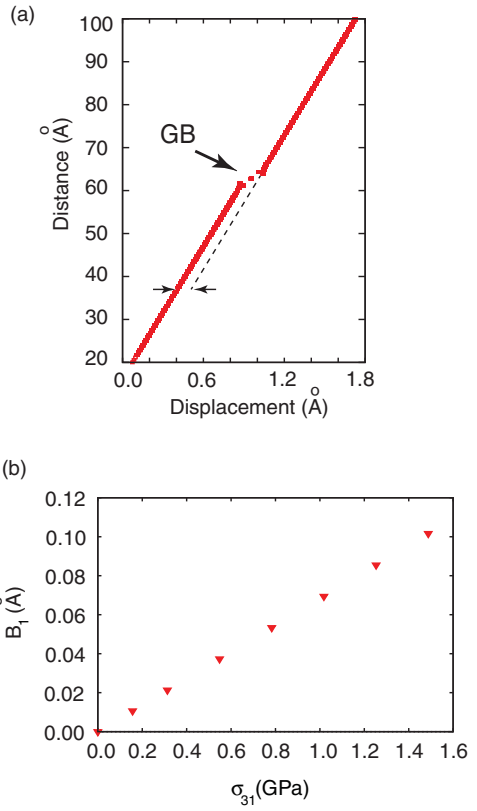

FIG. 9. (Color online) (a) Displacement u_1 of atoms in the direction parallel to the GB plane versus the distance normal to the GB. The applied shear stress is $\sigma_{31} = 1.5$ GPa and the temperature is 0 K. The relative shift of the horizontal segments of the plot is indicated. (b) Excess GB shear B_1 as a function of applied shear stress σ_{31}. Note that the stress-free value of B_1 is zero by the symmetry of the GB studied in this work.

shear strain e_{31} and is the same in both grains by crystal symmetry. Note the significant decrease of the slope in the GB core. This decrease creates a relative shift of the two linear segments and reflects the excess of shear in the GB. This plot demonstrates how the excess shear contributes to elastic response of the bicrystal. Weissmüller *et al.*[30] have recently developed a kinematic theory for the average excess shear in polycrystalline materials.

For a GB subject to the shear stress σ_{31}, Eq. (4) gives

$$\gamma = [U]_N/A - \sigma_{31} B_1, \tag{36}$$

where the second term accounts for the work done by the stress during the GB formation. The integrated form of the adsorption equation (6) is

$$\gamma = \gamma_0 - \int B_1 d\sigma_{31}. \tag{37}$$

The excess shear B_1 is plotted in Fig. 9(b) versus the shear stress σ_{31}. The obvious linearity of the plot indicates that the GB is deformed in a linear-elastic mode, with the stiffness coefficient of about 150 GPa/nm. The respective compliance coefficient is about 7 pm/GPa. By fitting a mechanical model to experimental data for nanocrystalline Pd,[31] Weissmüller *et al.*[30] have recently estimated the GB compliance coefficient to be 18 pm/GPa. The comparison is reasonable given that

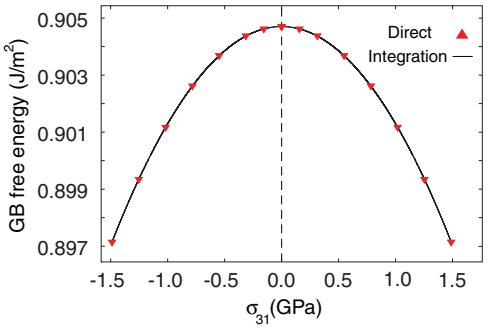

FIG. 10. (Color online) GB free energy γ as a function of shear stress σ_{31} parallel to the tilt axes at 0 K. The discrete points were obtained by direct calculations while the line by thermodynamic integration.

these numbers refer to different models, different materials, and a specific GB in our case and a polycrystalline material in the experiment.[31]

Figure 10 shows the GB free energy γ as a function of σ_{31} computed directly from Eq. (36) and by integration of Eq. (37). The symmetry of this GB dictates that γ should not depend on the sign of σ_{31}. It is therefore expected that γ should reach a maximum or minimum in the stress-free state. For this particular boundary, the stress-free state is a maximum, with γ slowly decreasing under stress. Considering that this effect is a higher order than linear, it is not surprising that γ is reduced by only 0.88% under the maximum stress of 1.5 GPa tested in this work.

4. *Maxwell relations*

There are six Maxwell relations that can be tested by simulations of pure Cu at 0 K. Three of them are satisfied automatically by the symmetry of the chosen GB, which dictates that both derivatives must be zero. Three remaining relations are nontrivial and permit testing by simulations. Each of these relations has a physical and a Lagrangian formulation, making the total of six relations. We will present tests of two of them in detail. Test of other Maxwell relations are summarized in Tables I (Lagrangian form) and II (physical form).

We first examine the Maxwell relation (18) in the physical form. The derivatives in this relation correspond to different uniaxial deformation paths described in Sec. IV A1. To

TABLE I. Derivatives involved in the Lagrangian form of the Maxwell relations (18)–(21) computed at 0 K. The expressions in the first row are the denominators of the partial derivatives, while the first column contains the numerators. The derivatives were evaluated for the state with stress-free grains. The table is symmetrical (within the accuracy of our calculations) in accord with predictions of the Maxwell relations. Some of the entries are zero due to the symmetry of the GB.

	$\partial\tau'_{11}$	$\partial\tau'_{22}$	$\partial B'_1$	$\partial([V]_N/A')$
∂e_{11}	...	0.0376 J/m^2	0.0	0.0114 nm
∂e_{22}	0.0376 J/m^2	...	0.0	0.03749 nm
$\partial\sigma_{31}$	0.0	0.0	...	0.0
$\partial\sigma_{33}$	−0.0113 nm	−0.03771 nm	0.0	–

TABLE II. Derivatives involved in the physical form of the Maxwell relations (18)–(21) computed at 0 K. The expressions in the first row are the denominators of the partial derivatives, while the first column contains the numerators. The derivatives were evaluated for the state with stress-free grains. The table is symmetrical (within the accuracy of our calculations) in accord with predictions of the Maxwell relations. Some of the entries are zero due to the symmetry of the GB.

	$\partial(\tau_{11}-\gamma)$	$\partial(\tau_{22}-\gamma)$	∂B_1	$\partial([V]_N/A)$
∂e_{11}	...	0.0159 J/m^2	0.0	0.0203 nm
∂e_{22}	0.0159 J/m^2	...	0.0	0.006086 nm
$\partial\sigma_{31}$	0.0	0.0	...	0.0
$\partial\sigma_{33}$	0.0203 nm	−0.006086 nm	0.0	–

compute these derivatives, we need to know τ_{ii} and γ as functions of e_{11} and e_{22} for these two paths. The calculations were performed using Eqs. (29) and (33) for each deformed state of the boundary. The obtained $(\tau_{11}-\gamma)$ and $(\tau_{22}-\gamma)$ are plotted as functions of the strains e_{22} and e_{11} in Figs. 11(a) and 11(b), respectively. The discrete points correspond to separate simulations for different strains. The dashed lines are tangents to the plots representing the computed derivatives at zero strain. The derivatives were found to be 0.0159 J/m^2 for both plots. Thus the Maxwell relation (18) holds within the accuracy of our calculations.

In the second example, we test the relation (19), this time in the Lagrangian form. To evaluate the derivative in the left-hand side, τ'_{11} was computed as a function of σ_{33} for the elastic

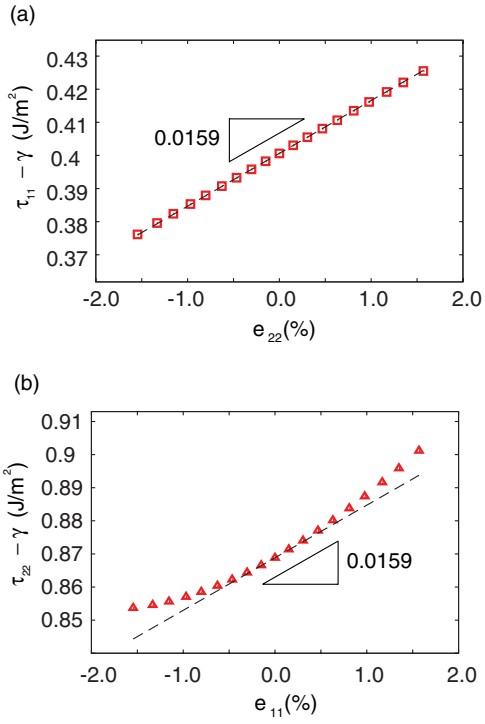

FIG. 11. (Color online) Test of the Maxwell relation (18) in the physical form. The points represent calculations for individual strains at 0 K. The dashed lines are slopes to the plots of (a) $(\tau_{11}-\gamma)$ versus e_{22} and (b) $(\tau_{22}-\gamma)$ versus e_{11} at zero stress. The right triangles with the slopes of 0.0159 J/m^2 are shown as a guide to eye.

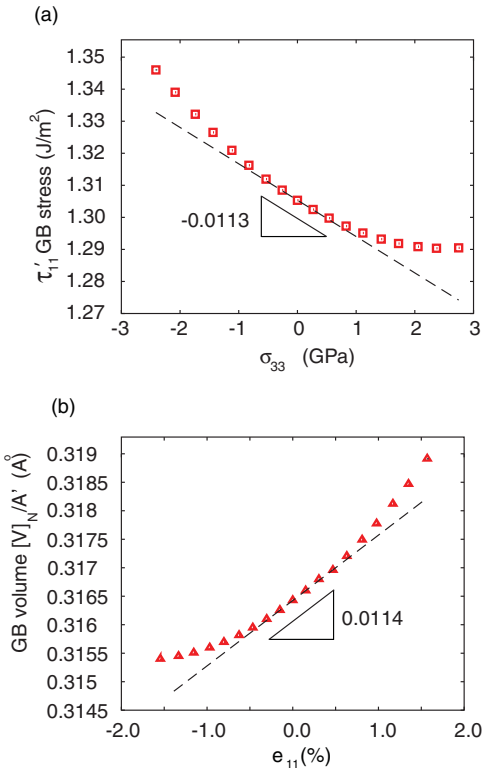

FIG. 12. (Color online) Test of the Maxwell relation (19) in the Lagrangian form. The points represent calculations for individual strains at 0 K. The dashed lines are slopes to the plots of (a) τ'_{11} versus σ_{33} and (b) $[V]_N/A'$ versus e_{11}. The right triangles with the slopes of -0.0113 and 0.0114 nm, respectively, are shown as a guide to the eye.

deformation described in Sec. IV A2. For the derivative in the right-hand side, the excess GB volume was computed as a function of e_{11} (see Sec. IV A1) and normalized by the stress-free GB area A'. The respective plots are shown in Fig. 12. The derivatives evaluated at zero stress were found to be -0.0113 nm and 0.0114 nm, respectively, which is in excellent agreement with prediction of Eq. (19).

B. Pure Cu at finite temperatures

For a single-component GB with stress-free grains at finite temperatures, Eq. (4) gives the GB free energy

$$\gamma A = [U]_N - T[S]_N. \tag{38}$$

Because the excess entropy $[S]_N$ cannot be easily computed by MD simulations, γ was calculated by thermodynamic integration of the Gibbs-Helmholtz equation (10), which does not contain $[S]_N$. We chose the integration path on which temperature varies, σ_{31} and σ_{33} remain zero, and the lateral strain is adjusted to accommodate the thermal expansion of the lattice. For this path, the integrated form of Eq. (10) is

$$\gamma A = \frac{(\gamma_0 A_0)T}{T_0} - T\int_{T_0}^{T}\left(\frac{[U]_N}{T^2} - \frac{(\tau_{11}+\tau_{22})A}{T}\frac{de}{dT}\right)dT. \tag{39}$$

Here, e is the biaxial lateral strain and the derivative de/dT is the thermal expansion coefficient of the stress-free Cu lattice.

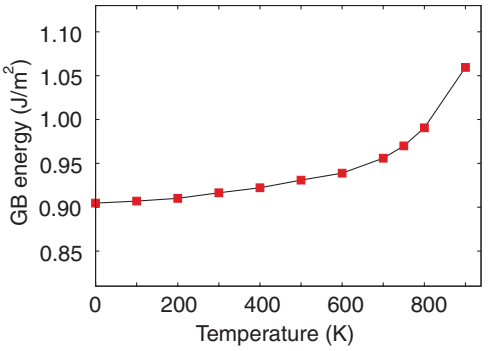

FIG. 13. (Color online) Excess GB energy $[U]_N/A$ as a function of temperature for stress-free grains in pure Cu. The points were obtained by MD simulations and are connected by lines as a guide to the eye.

The quantities γ_0, A_0, and T_0 are the GB free energy, area, and temperature corresponding to the reference state, respectively. The excess quantities $[U]_N$ and τ_{ii} involved in Eq. (39) were computed for a discrete set of temperatures along the path and are presented in Figs. 13 and 14, respectively. Note that the GB stress τ_{ii} is anisotropic at all temperatures along the path, with both components decreasing with temperature.

The solid line in Fig. 15 indicates the GB free energy γ computed from Eq. (39) as a function of temperature. The reference temperature $T_0 = 300$ K was used and the integration was performed to temperatures both below and above T_0. The two points on the plot indicate the values of γ at 0 K and at 300 K. The reference value γ_0 was obtained by quasiharmonic calculations,[28] whereas the 0 K value was computed directly by Eq. (29). Observe that the integration towards 0 K gives exactly the number obtained by the direct calculation, which validates our methodology. Over the entire temperature range studied here, γ decreases from 0.905 J/m^2 at 0 K to 0.660 J/m^2 at 900 K. The trend for γ to decrease with temperature is consistent with previous simulations.[32,33]

C. Cu-Ag alloys at finite temperatures

Figure 16 shows MC snapshots of the simulation block with the grain compositions of 0.036%, 0.24%, and 0.58% Ag at 800 K. These images demonstrate that Ag strongly

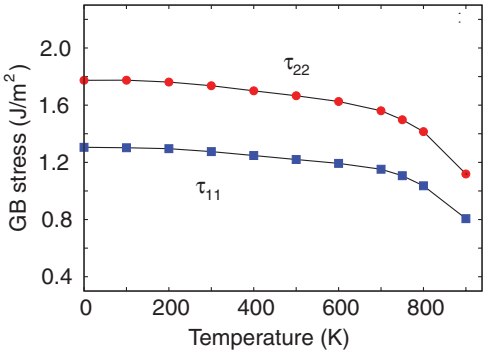

FIG. 14. (Color online) GB stress components τ_{11} and τ_{22} as functions of temperature for stress-free grains in pure Cu. The points were obtained by MD simulations and are connected by lines as a guide to the eye.

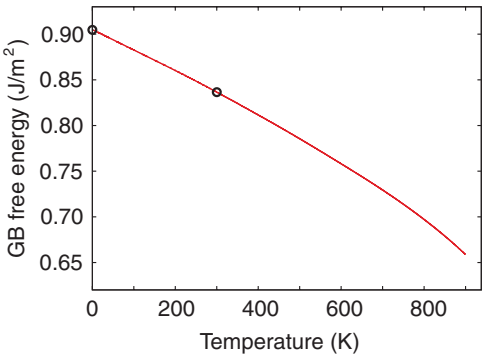

FIG. 15. (Color online) GB free energy γ as a function of temperature for stress-free grains in pure Cu. The line was computed by thermodynamic integration while the points represent direct calculations at the reference temperature of $T_0 = 300$ K and at 0 K.

segregates to the GB and that the segregated amount and the width of the segregation region both increase with temperature. It is also apparent that at the highest Ag concentrations studied here, the boundary becomes visibly disordered. In Fig. 17, we plot the excess GB volume per unit area as a function of grain composition. The discrete points on the plot represent individual MC runs at particular values of the imposed diffusion potential M_{21}. The excess GB volume monotonically increases with c_{Ag} and becomes nearly four times the value in pure Cu when c_{Ag} reaches the maximum concentration of 0.58%. This increase is consistent with the larger size of Ag atoms in comparison with Cu atoms. Note that the slope of the plot increases at high concentrations when the boundary develops the atomic disorder.

For the simulation conditions discussed here, Eq. (4) gives the GB free energy

$$\gamma A = [U]_N - T[S]_N - [N_2]_N M_{21}. \tag{40}$$

To circumvent a calculation of $[S]_N$, γ was computed as a function of c_{Ag} by integration of the adsorption equation with

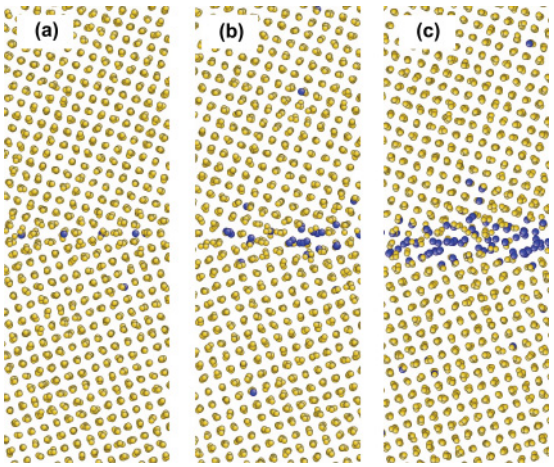

FIG. 16. (Color online) Snapshots of the Cu-Ag simulation block with the GB concentration of silver c_{Ag} (a) 0.036%, (b) 0.24%, and (c) 0.58% at $T = 800$ K. Cu atoms are shown in yellow and Ag atoms in dark blue. The images were produced with the ATOMEYE visualization program.[43]

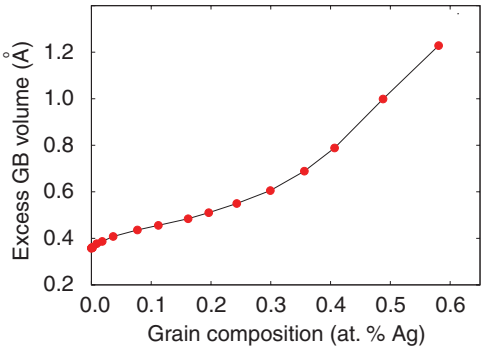

FIG. 17. (Color online) Excess GB volume per unit area, $[V]_N/A$, as a function of the silver concentration in the grains at a fixed temperature of 800 K. The points were obtained by MC simulations and are connected by lines as a guide to the eye.

respect to c_{Ag} from the pure copper state ($c_{\mathrm{Ag}} = 0$) to the current composition. The value of γ for pure Cu was taken from the MD simulations discussed in Sec. IV B. On this integration path, the temperature remains fixed at 800 K, the grains are stress-free, and M_{21} is varied to gradually increase the concentration of Ag. The lateral dimensions of the system are also varied due to the compositional strain.[6,7,34] For this path, the integrated form of Eq. (6) is

$$\gamma A = \gamma_0 A_0 - \int_0^{c_{\mathrm{Ag}}} \left\{ [N_2]_N \frac{dM_{21}}{dc_{\mathrm{Ag}}} + (\tau_{11} + \tau_{22}) A \frac{de}{dc_{\mathrm{Ag}}} \right\} dc_{\mathrm{Ag}}, \tag{41}$$

where the derivative de/dc_{Ag} represents the change in the stress-free lattice constant with composition.

The GB excesses entering Eq. (41) were computed as functions of composition and are shown in Figs. 18 and 19. As already expected from the images in Fig. 16, the GB segregation $[N_2]_N/A$ increases with the grain composition (see Fig. 18). In the composition range where the boundary preserves its relatively ordered structure, the shape of the segregation curve is qualitatively consistent with the Langmuir–McLean isotherm.[1] At higher Ag concentrations when the

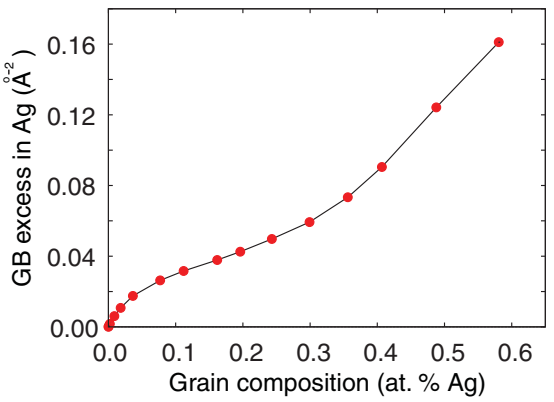

FIG. 18. (Color online) GB segregation $[N_2]_N/A$ as a function of the grain composition c_{Ag} at a fixed temperature of 800 K. The points were obtained by MC simulations and are connected by lines as a guide to the eye.

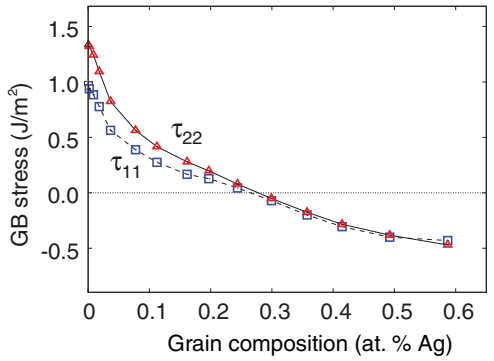

FIG. 19. (Color online) The components τ_{11} and τ_{22} of the GB stress tensor as functions of the grain composition c_{Ag} at a fixed temperature of 800 K. The points were obtained by MC simulations and are connected by lines as a guide to the eye.

GB becomes more disordered, the slope of the segregation isotherm increases, indicating an increased capacity of this GB to absorb Ag atoms. Figure 19 shows the GB stress components τ_{11} and τ_{22} as functions of c_{Ag}. Both components decrease with concentration and eventually merge, making the GB stress tensor virtually isotropic. Note the change of sign of τ_{ii} at $c_{Ag} \approx 0.28\%$, indicating that the GB is under tension below this composition and under compression above. A similar reversal of sign of GB stress with alloy composition was observed experimentally in the Pd-H system.[35,36] The experiments also revealed a correlation between the GB excess volume and segregation.[35] The two systems are very different in both thermodynamics and the mechanism solubility (interstitial mechanism in Pd-H, substitutional in Cu-Ag). It can be noted, however, that the interstitial hydrogen and the "oversized" substitutional Ag atoms both produce compressive stresses in the lattice and can be expected to increase the GB excess volume when segregation occurs.

Finally, the GB free energy γ computed by thermodynamic integration (41) is plotted versus c_{Ag} in Fig. 20. The plot shows the expected decrease of γ with alloying and is convex at small concentrations in agreement with the Langmuir–McLean isotherm. At higher concentrations the plot turns over and becomes concave. This change of shape reflects the positive deviation of the segregation isotherm from the Langmuir–McLean form (cf. Fig. 18), causing the more rapid decrease of γ. Overall, the GB free energy decreases at this temperature from $\gamma = 0.70$ J/m^2 for pure Cu to $\gamma = 0.54$ J/m^2 at $c_{Ag} = 0.58\%$.

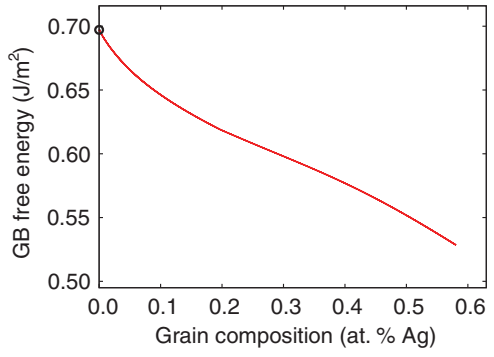

FIG. 20. (Color online) GB free energy γ computed by thermodynamic integration as a function of the grain composition c_{Ag} at a fixed temperature of 800 K. The point at $c_{Ag} = 0$ represents the GB free energy in pure Cu used as the reference value.

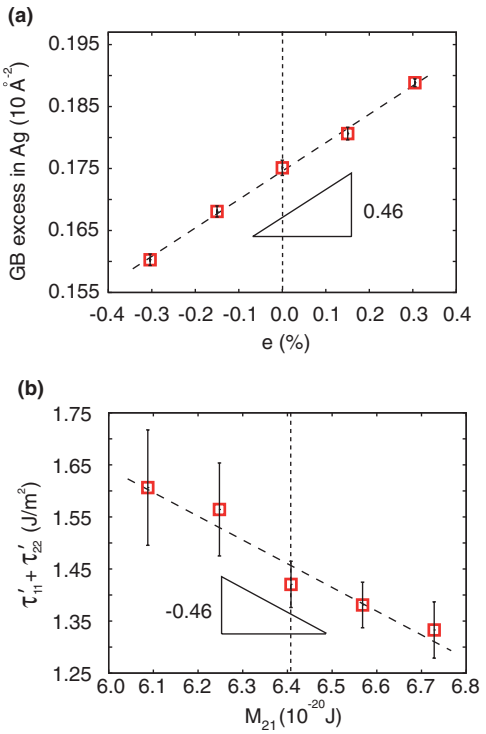

FIG. 21. (Color online) Test of the Lagrangian form of the Maxwell relation (22) for the GB in the binary Cu-Ag solution at 800 K. The discrete points represent MC simulation data. (a) GB segregation $[N_2]_N/A'$ as a function of biaxial strain parallel to the boundary. (b) Sum of the principal components, τ'_{11} and τ'_{22}, of the GB stress tensor as a function of the diffusion potential M_{21}. The slopes of the dashed lines represent the derivatives appearing in the Maxwell relation. The vertical dashed lines indicate the state in which the derivatives are taken, i.e., stress-free grains with the chemical composition of $c_{Ag} = 0.036\%$. The right triangles with the slopes of 0.46 and -0.46 Å^{-2}, respectively, are shown as a guide to the eye.

D. Effects of elastic deformation and temperature on segregation

The MC simulations were also used to study the effect of elastic deformation, parallel, and normal to the GB plane, and temperature on GB segregation. These effects are expressed by appropriate Maxwell relations, which were used in the Lagrangian form in order to avoid a calculation of γ as a function of respective intensive variables.

The effect of elastic deformation parallel to the GB plane was modeled by applying a biaxial strain e. For this type of deformation, the Maxwell relation (22) predicts

$$\frac{\partial(\tau'_{11} + \tau'_{22})}{\partial M_{21}} = -\frac{\partial([N_2]_N/A')}{\partial e}. \qquad (42)$$

Figure 21(a) shows the GB segregation per unit reference area as a function of strain e computed at constant M_{21} and zero σ_{31} and σ_{33}. The total amount of segregation increases linearly with strain in this deformation range. As expected, tension favors the segregation of larger Ag atoms. Figure 21(b) shows that the sum of the GB stress components decreases with M_{21} (i.e., with increasing c_{Ag}), which is again consistent with the atomic size effect. The computed derivatives appearing in Eq. (42) are -0.46 ± 0.08 Å^{-2} in the left-hand side and 0.46 ± 0.01 Å^{-2} in the right-hand side. They are opposite in sign and equal in magnitude within the error bars in agreement with Eq. (42).

Secondly, we examined the effect of the normal stress σ_{33} on segregation and tested the Maxwell relation (23). According to this relation, the effect of σ_{33} on segregation is related to the change in the GB excess volume with M_{21}. Figure 22(a) shows the segregation $[N_2]_N/A'$ as a function of σ_{33} at fixed lateral dimensions of the simulation block, constant value of M_{21} and zero σ_{31}. As expected from the atomic size effect, the segregation increases under tension ($\sigma_{33} > 0$) and decreases under compression ($\sigma_{33} < 0$). Similarly, the GB excess volume increases with increasing M_{21} (and thus c_{Ag}) [see Fig. 22(b)]. The respective derivatives are found to be 0.027 ± 0.004 Å^{-2}GPa^{-1} in the left-hand side and 0.030 ± 0.0006 Å^{-2} GPa^{-1} in the right-hand side. Within the error bars, these derivatives are equal in agreement with Eq. (23).

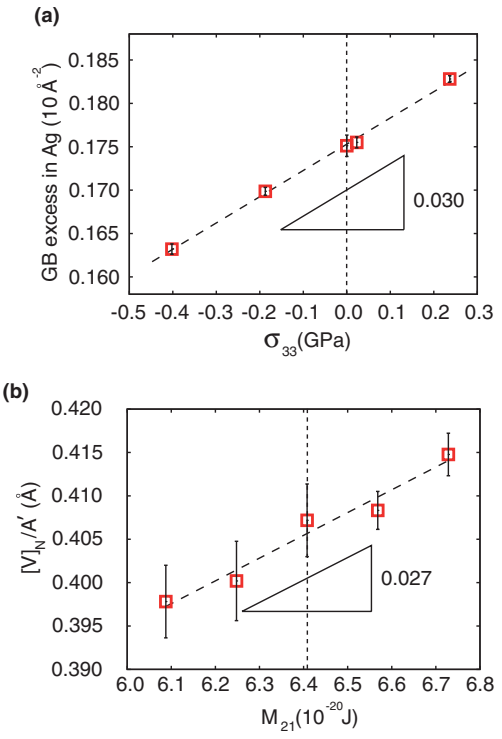

FIG. 22. (Color online) Test of the Lagrangian form of the Maxwell relation (23) for the GB in the binary Cu-Ag solution at 800 K. The discrete points represent MC simulation data. (a) GB segregation $[N_2]_N/A'$ as a function of normal stress σ_{33}. (b) Excess volume $[V]_N/A'$ as a function of the diffusion potential M_{21}. The slopes of the dashed lines represent the derivatives appearing in the Maxwell relation. The vertical dashed lines indicate the state in which the derivatives are taken, i.e., stress-free grains with the chemical composition of $c_{Ag} = 0.036\%$. The right triangles with the slopes of 0.030 and 0.027 Å^{-2} GPa^{-1}, respectively, are shown as a guide to the eye.

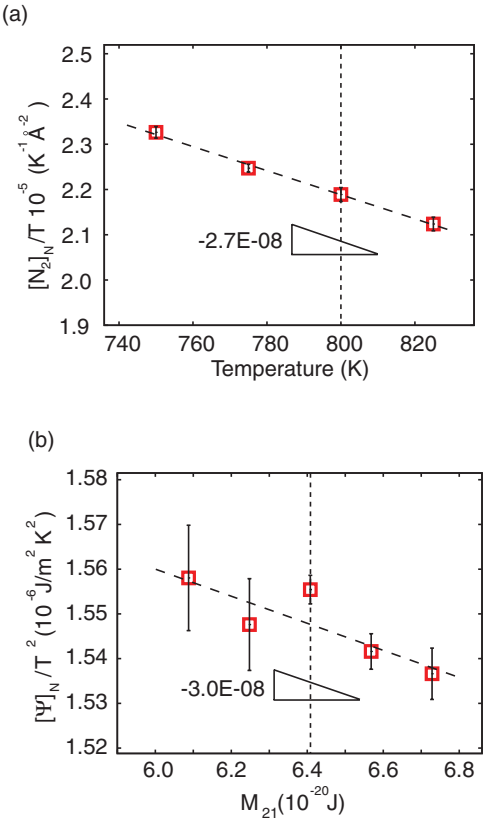

FIG. 23. (Color online) Test of the Lagrangian form of the Maxwell relation (28) for the GB in the binary Cu-Ag solution at 800 K. The discrete points represent MC simulation data. (a) GB segregation $[N_2]_N/A'$ as a function of temperature. (b) The potential $[\Psi]_N/A'T^2$ as a function of the diffusion potential M_{21}. The slopes of the dashed lines represent the derivatives appearing in the Maxwell relation. The vertical dashed lines indicate the state in which the derivatives are taken, i.e., stress-free grains with the chemical composition of $c_{Ag} = 0.036\%$. The right triangles with the slopes of -2.7×10^{-8} and -3.0×10^{-8} Å^{-2} K^{-2}, respectively, are shown as a guide to the eye.

Finally, we tested Eq. (28) which involves the change in segregation with temperature. Fig. 23 displays $[N_2]_N/A'T$ and $[\Psi]_N/A'T^2$ as a functions of T and M_{21}, respectively. These variations occur at zero σ_{31} and σ_{33} and fixed GB area. According to Eq. (11), the potential Ψ reduces to $[U]_N - [N_2]_N M_{21}$. Within the accuracy of our calculations, the obtained derivatives, $-(2.7 \pm 0.1) \times 10^{-8}$ Å^{-2} K^{-2} in the left-hand side and $-(3.0 \pm 0.9) \times 10^{-8}$ Å^{-2} K^{-2} in the right-hand side, are equal as predicted by Eq. (28).

The effect of the shear stress σ_{31} on segregation is expected to be a second- or higher-order effect for this GB and was not studied here.

V. DISCUSSION AND CONCLUSIONS

Thermodynamic properties of GBs play an important role in many materials processes. The GB free energy controls the

driving force of grain coarsening and affects the barriers of phase nucleation.[1,2,37] The GB stress affects internal stresses in nanocrystalline materials[30,35,38,39] and their chemical reactivity. GB segregation can drastically change mechanical properties of polycrystalline materials.[1,2] Some phenomena can be caused by cross effects, such as the effect of elastic stresses on GB segregation and segregation on elastic compliance of the material. Experimental studies of GB thermodynamics are invaluable but rare, difficult and usually provide information averaged over multiple GBs. Critical insights can be gained by atomistic simulations of individual GBs with precisely known crystallography, structure and chemical composition.

Although real materials are often subject to mechanical loads, thermodynamic calculations are usually focused on GBs between stress-free grains. It is straightforward to apply a stress to a GB in atomistic simulations. The main obstacle has been the absence of a thermodynamic framework for calculations of GB properties under stress. The existing thermodynamic theories either disregard the stresses altogether or consider only a hydrostatic state of stress. In the latter case, the GBs are treated essentially the same way as interfaces in fluid systems. It has not been known how to compute, or even properly define, the GB free energy, GB stress, and other excess properties when the GB is subject to nonhydrostatic stresses.

In this work, we applied the thermodynamic theory of coherent interfaces[3] to coherent GBs in the presence of nonhydrostatic stresses. The equations of Ref. 3 were adapted to GBs in two ways. Firstly, the fact that the system contains only one phase was taken into account. This significantly simplified the calculations. In particular, the interface excess quantities are now defined through 2×2 determinants which can be transformed to simpler and more intuitive expressions. Secondly, the GB theory recognizes that for the system to remain a single phase under applied stresses, both the stress tensor and the GB itself must possess certain symmetries. Such symmetries must be identified and formulated as appropriate constrains imposed on possible state variations.

The GB free energy γ has been defined as the reversible work of GB formation under an applied nonhydrostatic stress. Equation (4) expresses γ through appropriate excesses of extensive properties and contains a term accounting for the work of the applied stress. This term includes the work of the shear stress parallel to the boundary plane, which exists only for coherent GBs (i.e., when the shear stresses causes an elastic response of the boundary and not GB sliding). Furthermore, our definition of γ contains only the diffusion potentials of substitutional components, avoiding chemical potentials that are undefined quantities in nonhydrostatic solids. It is only for hydrostatic grains that γ can be expressed through chemical potentials as indicated in Eq. (5).

Two forms of the generalized adsorption equation have been presented in this work: the standard (6) and the Gibbs-Helmholtz (10) forms. The differential coefficients of these equations define the GB excesses which are physically meaningful and, in principle, measurable quantities. Along with the already known excesses such as the GB segregation, GB stress, and and GB excess volume, the generalized adsorption equation introduces the excess GB shear. The additional term containing the GB shear did not exist in previous formulations of the adsorption equation for GBs.[8] It has naturally appeared in our formulation due to the incorporation of the applied shear stress. As mentioned earlier, the existence of excess shear was recognized in previous mechanical theories of interfaces and was referred to as "slip."[30,35,38] However, this quantity was not associated with an additional term in the adsorption equation. (See Ref. 3 for a discussion of the thermodynamic approach developed in this work in comparison with previous mechanical theories of interfaces.[30,35,38,40,41])

The Gibbs-Helmholtz form (10) of the adsorption equation affords efficient numerical calculations of γ by thermodynamic integration starting from a state for which γ is known. This integration requires knowledge of the readily accessible excess quantities along the integration path, such as the excess energy, the amount of segregation and the GB stress. Equation (7) provides a numerical recipe for calculations of the GB stress as an appropriate excess of the lateral stress components. Despite the critical importance of the GB free energy, only a few previous calculations were performed for finite temperatures[32,33] and none for stressed grains.

The generalized adsorption equation generates a number of Maxwell relations between its differential coefficients. These relations describe a variety of cross effects between segregation, stresses, strains, temperature, and other parameters. They describe physically measurable effects, some of which can be practically important. As one example, Eq. (24) predicts a relation between the effect of an applied shear stress on GB segregation, on one hand, and the response of the excess shear to changes in the diffusion potential, on the other hand. The diffusion potential can be controlled by varying the chemical composition of the material.

The proposed theory has been applied to atomistic simulations of the symmetrical tilt $\Sigma 5\,(310)\,[001]$ GB in Cu and Cu-Ag alloys. Accurate atomistic potentials have been used, making these simulations relevant to real materials. A combination of MD and MC methods has been applied to study the effects of elastic deformation, chemical composition and temperature on GB properties. Along with providing useful information about typical orders of magnitude of the effects, these simulations also served as a test bed of the theory. A number of cross-checks have been made by comparing different calculations of the same physical quantity. For example, the GB free energy computed by thermodynamic integration was compared with results of direct calculations at 0 K. As another example, several Maxwell relations have been tested by separate calculations of the derivatives appearing in the right-hand and left-hand sides. Excellent agreement was invariably found in all tests, giving us confidence in the correctness of the proposed thermodynamic equations and the accuracy of our simulations.

The simulations have also demonstrated that the effects of elastic stresses, temperature and segregation on the GB free energy can be significant. These effects could compromise the accuracy of many simplified theories involving GB processes. For example, in the classical theory of heterogeneous nucleation at GBs, γ is assumed to be constant. Variations of γ with temperature, segregation and applied stresses can significantly impact the nucleation barriers and thus the predicted nucleation rates. It should be noted that some of the GB properties are affected by variations in temperature and chemical composition stronger than γ. For example, the

excess GB volume increases a factor of four and the GB stress changes its sign with the introduction of less than one atomic percent of Ag in Cu.

Finally, it should be recognized that some aspects of our simulations are specific to the particular $\Sigma 5$ GB chosen for this work. This boundary has a mirror symmetry across the plane normal to the tilt axis, as do most of other symmetrical tilt GBs. Due to this symmetry, (i) the stress-free value of the excess GB shear along the tilt axis is zero [see Fig. 9(b)] and (ii) thermodynamic properties of this GB do not depend on the sign of the shear stress σ_{31} applied parallel to the tilt axis. As a result, the effect of σ_{31} on γ and other GB properties is quadratic in stress, see example in Fig. 10. This is in contrast to the excess volume, which has a finite value for stress-free grains (see Fig. 7) and produces a linear response of GB properties to σ_{33} [see examples in Figs. 8 and 12(a)]. For GBs that do not possess the mentioned mirror symmetry, the response to the shear stress can be linear and thus stronger. For example, the symmetrical tilt $\Sigma 13\,(3\bar{4}1)\,[111]$ GB in Al studied by atomistic simulations[42] shows a 0.2 Å shift of one grain relative to the other parallel to the tilt axis [111]. This nonzero shift is an intrinsic structural property of this GB and constitutes its stress-free excess shear. It preserves the twofold symmetry of the GB structure around the x_2 axis, so that the boundary can still support an applied shear stress σ_{31}. Due to this nonzero shift, the response of the GB properties to σ_{31} is expected to be linear, a prediction which could be tested by simulations. The interplay between GB thermodynamics and crystal symmetry is an interesting subject that deserves a more detailed study in the future.

ACKNOWLEDGMENTS

This work was supported by the US Department of Energy, Office of Basic Energy Sciences, the Physical Behavior of Materials Program, under Grant No. DE-FG02-01ER45871.

*tfrolov@gmu.edu
†ymishin@gmu.edu

[1] A. P. Sutton and R. W. Balluffi, *Interfaces in Crystalline Materials* (Clarendon Press, Oxford, 1995).
[2] Y. Mishin, M. Asta, and J. Li, Acta Mater. **58**, 1117 (2010).
[3] T. Frolov and Y. Mishin, Phys. Rev. B **85**, 224106 (2012).
[4] J. W. Cahn, Y. Mishin, and A. Suzuki, Acta Mater. **54**, 4953 (2006).
[5] J. W. Gibbs, *The Collected Works of J. W. Gibbs* (Yale University Press, New Haven, 1948), Vol. 1.
[6] F. C. Larchè and J. W. Cahn, Acta Metall. **26**, 1579 (1978).
[7] F. C. Larchè and J. W. Cahn, Acta Metall. **33**, 331 (1985).
[8] J. W. Cahn, in *Interface Segregation*, edited by W. C. Johnson and J. M. Blackely (American Society of Metals, Metals Park, OH, 1979), Chap. 1, pp. 3–23.
[9] L. Shvindlerman and G. Gottstein, Scri. Mater. **54**, 1041 (2006).
[10] L. S. Shvindlerman, G. Gottstein, V. A. Ivanov, D. A. Molodov, D. Kolesnikov, and W. Łojkowski, J. Mater. Sci. **41**, 7725 (2006).
[11] E. M. Steyskal, B. Oberdorfer, W. Sprengel, M. Zehetbauer, R. Pippan, and R. Würschum, Phys. Rev. Lett. **108**, 055504 (2012).
[12] H. Zhang and D. J. Srolovitz, Acta Mater. **54**, 623 (2006).
[13] M. A. Tschopp, G. J. Tucker, and D. L. McDowell, Acta Mater. **55**, 3959 (2007).
[14] D. L. Olmsted, S. M. Foiles, and E. A. Holm, Acta Mater. **57**, 3694 (2009).
[15] T. Frolov and Y. Mishin, Modell. Simul. Mater. Sci. Eng. **18**, 074003 (2010).
[16] L. D. Landau and E. M. Lifshitz, *Statistical Physics, Part I*, 3rd ed. (Butterworth-Heinemann, Oxford, 2000).
[17] L. E. Malvern, *Introduction To The Mechanics Of A Continuous Medium* (Prentice-Hall, Upper Saddle River, 1969).
[18] R. Shuttleworth, Proc. Phys. Soc. **63**, 444 (1949).
[19] A. Suzuki and Y. Mishin, Interface Sci. **11**, 131 (2003).
[20] T. Gorkaya, D. A. Molodov, and G. Gottstein, Acta Mater. **57**, 5396 (2009).
[21] Y. Mishin, M. J. Mehl, D. A. Papaconstantopoulos, A. F. Voter, and J. D. Kress, Phys. Rev. B **63**, 224106 (2001).
[22] P. L. Williams, Y. Mishin, and J. C. Hamilton, Modell. Simul. Mater. Sci. Eng. **14**, 817 (2006).
[23] *Binary Alloy Phase Diagrams*, edited by T. B. Massalski (ASM, Materials Park, OH, 1986).
[24] [http://www.itap.physik.uni-stuttgart.de/imd/].
[25] J. Roth, F. Gähler, and H.-R. Trebin, Int. J. Mod. Phys. C **11**, 317 (2000).
[26] J. Stadler, R. Mikulla, and H. R. Trebin, Int. J. Mod. Phys. C **8**, 1131 (1997).
[27] S. M. Foiles, Phys. Rev. B **32**, 7685 (1985).
[28] S. M. Foiles, Phys. Rev. B **49**, 14930 (1994).
[29] D. Frenkel and B. Smit, *Understanding Molecular Simulation: From Algorithms to Applications*, 2nd ed. (Academic, San Diego, 2002).
[30] J. Weissmüller, J. Markmann, M. Grewer, and R. Birringer, Acta Mater. **59**, 4366 (2011).
[31] M. Grewer, J. Markman, R. Karos, and W. A. R. Birringer, Acta Mater. **59**, 1523 (2011).
[32] J. Q. Broughton and G. H. Gilmer, Phys. Rev. Lett. **56**, 2692 (1986).
[33] S. M. Foiles, Scr. Mater. **62**, 231 (2010).
[34] F. Larchè and J. W. Cahn, Acta Metall. **21**, 1051 (1973).
[35] C. Lemier and J. Weissmuller, Acta Mater. **55**, 1241 (2007).
[36] R. Birringer, M. Hoffmann, and P. Zimmer, Phys. Rev. Lett. **88**, 206104 (2002).
[37] T. Frolov and Y. Mishin, Phys. Rev. Lett. **106**, 155702 (2011).
[38] M. E. Gurtin, J. Weissmuller, and F. Larchè, Philos. Mag. A **78**, 1093 (1998).
[39] D. Kramer and J. Weissmuller, Surface Sci. **601**, 3042 (2007).
[40] M. E. Gurtin and A. I. Murdoch, Arch. Ration. Mech. Anal. **57**, 291 (1975).
[41] E. Fried and M. E. Gurtin, J. Stat. Phys. **95**, 1361 (1999).
[42] A. Suzuki and Y. Mishin, Interface Science **11**, 425 (2003).
[43] J. Li, Modell. Simul. Mater. Sci. Eng. **11**, 173 (2003).
[44] It is worth reminding that, although we keep both terms $AB_1 d\sigma_{31}$ and $AB_2 d\sigma_{32}$ in Eq. (6) for the sake of generality, for every particular GB subject to shear stresses only one of such terms actually enters this equations. The other term vanishes for the reasons discussed in Sec. V B of Part I.[3]